

1 **MitoChime: A Machine Learning Pipeline for**
2 **Detecting PCR-Induced Chimeras in**
3 **Mitochondrial Illumina Reads**

4 A Special Project Proposal
5 Presented to
6 the Faculty of the Division of Physical Sciences and Mathematics
7 College of Arts and Sciences
8 University of the Philippines Visayas
9 Miagao, Iloilo

10 In Partial Fulfillment
11 of the Requirements for the Degree of
12 Bachelor of Science in Computer Science

13 by

14 Duranne Duran
15 Yvonne Lin
16 Daniella Pailden

17 Adviser
18 Francis D. Dimzon, Ph.D.

19 December 5, 2025

Abstract

21 Next-generation sequencing (NGS) platforms have advanced research but re-
22 main susceptible to artifacts such as PCR-induced chimeras that compromise
23 mitochondrial genome assembly. These artificial hybrid sequences are prob-
24 lematic for small, circular, and repetitive mitochondrial genomes, where they
25 can generate fragmented contigs and false junctions. Existing detection tools,
26 such as UCHIME, are optimized for amplicon-based microbial community ana-
27 lysis and depend on reference databases or abundance assumptions unsuitable
28 for organellar assembly. To address this gap, this study presents MitoChime,
29 a machine learning pipeline for detecting PCR-induced chimeric reads in *Sar-*
30 *dinella lemuru* Illumina paired-end data without relying on external reference
31 databases.

32 Using simulated datasets containing clean and chimeric reads, a feature
33 set was extracted, combining alignment-based metrics (e.g., supplementary
34 alignments, soft-clipping) with sequence-derived statistics (e.g., k-mer com-
35 position, microhomology). A comparative evaluation of supervised learning
36 models identified tree-based ensembles CatBoost and Gradient Boosting as top
37 performers, achieving an F1-score of 0.77 and an ROC-AUC of 0.84 on held-
38 out test data. Feature importance analysis highlighted soft-clipping and k-mer
39 compositional shifts as the strongest predictors of chimerism, whereas micro-
40 homology contributed minimally. Integrating MitoChime as a pre-assembly
41 step can aid in streamlining mitochondrial reconstruction pipelines.

42 **Keywords:** Chimera detection, Mitochondrial genome,
Assembly, Machine learning

⁴³ **Contents**

⁴⁴	1 Introduction	1
⁴⁵	1.1 Overview	1
⁴⁶	1.2 Problem Statement	3
⁴⁷	1.3 Research Objectives	3
⁴⁸	1.3.1 General Objective	3
⁴⁹	1.3.2 Specific Objectives	4
⁵⁰	1.4 Scope and Limitations of the Research	4
⁵¹	1.5 Significance of the Research	6
⁵²	2 Review of Related Literature	7
⁵³	2.1 The Mitochondrial Genome	7
⁵⁴	2.1.1 Mitochondrial Genome Assembly	8

55	2.2 PCR Amplification and Chimera Formation	8
56	2.3 Existing Traditional Approaches for Chimera Detection	10
57	2.3.1 UCHIME	11
58	2.3.2 UCHIME2	12
59	2.3.3 CATch	13
60	2.3.4 ChimPipe	14
61	2.4 Machine Learning Approaches for Chimera and Sequence Quality	
62	Detection	14
63	2.4.1 Feature-Based Representations of Genomic Sequences . . .	15
64	2.5 Synthesis of Chimera Detection Approaches	16
65	3 Research Methodology	19
66	3.1 Research Activities	19
67	3.1.1 Data Collection	20
68	3.1.2 Feature Extraction Pipeline	23
69	3.1.3 Machine Learning Model Development	26
70	3.1.4 Model Benchmarking, Hyperparameter Optimization, and	
71	Evaluation	27
72	3.1.5 Feature Importance and Interpretation	28

73	3.1.6 Validation and Testing	29
74	3.1.7 Documentation	30
75	3.2 Calendar of Activities	31
76	4 Results and Discussion	32
77	4.1 Descriptive Analysis of Features	32
78	4.1.1 Exploratory Data Analysis	33
79	4.2 Baseline Classification Performance	34
80	4.3 Effect of Hyperparameter Tuning	36
81	4.4 Detailed Evaluation of Representative Models	37
82	4.4.1 Confusion Matrices and Error Patterns	38
83	4.4.2 ROC and Precision–Recall Curves	39
84	4.5 Feature Importance	40
85	4.5.1 Permutation Importance of Individual Features	40
86	4.5.2 Feature Family Importance	42
87	4.6 Summary of Findings	44
88	A Exploratory Data Analysis	46
89	A.1 Histograms of Key Features	46

⁹⁰ List of Figures

⁹¹	3.1 Process Diagram of Special Project	20
⁹²	4.1 Feature correlation heatmap showing relationships among alignment-derived and sequence-derived features.	34
⁹³		
⁹⁴	4.2 Test F1 of all baseline classifiers, showing that no single model clearly dominates and several achieve comparable performance. . .	35
⁹⁵		
⁹⁶	4.3 Comparison of test F1 (left) and ROC–AUC (right) for baseline and tuned models.	37
⁹⁷		
⁹⁸	4.4 Confusion matrices for the four representative models on the held-out test set.	39
⁹⁹		
¹⁰⁰	4.5 ROC (left) and precision–recall (right) curves for the four representative models on the held-out test set.	40
¹⁰¹		
¹⁰²	4.6 Permutation-based feature importance for four representative classifiers.	42
¹⁰³		
¹⁰⁴	4.7 Aggregated feature family importance across four models.	44

107 List of Tables

₁₁₂ **Chapter 1**

₁₁₃ **Introduction**

₁₁₄ **1.1 Overview**

₁₁₅ The rapid advancement of next-generation sequencing (NGS) technologies has
₁₁₆ transformed genomic research by enabling high-throughput and cost-effective
₁₁₇ DNA analysis (Metzker, 2010). Among current platforms, Illumina sequencing
₁₁₈ remains the most widely adopted, capable of producing millions of short reads
₁₁₉ that can be assembled into reference genomes or analyzed for genetic variation
₁₂₀ (Bentley et al., 2008; Glenn, 2011). Despite its high base-calling accuracy,
₁₂₁ Illumina sequencing is prone to artifacts introduced during library preparation,
₁₂₂ particularly polymerase chain reaction (PCR)-induced chimeras, which are ar-
₁₂₃ tificial hybrid sequences that do not exist in the true genome (Judo, Wedel, &
₁₂₄ Wilson, 1998).

₁₂₅ PCR chimeras form when incomplete extension products from one template

anneal to an unrelated DNA fragment and are extended, creating recombinant reads (Qiu et al., 2001). In mitochondrial genome assembly, such artifacts are especially problematic because the mitochondrial genome is small, circular, and often repetitive (Boore, 1999; Cameron, 2014). Even a small number of chimeric or misjoined reads can reduce assembly contiguity and introduce false junctions during organelle genome reconstruction (Dierckxsens, Mardulyn, & Smits, 2017; Hahn, Bachmann, & Chevreux, 2013; Jin et al., 2020). Existing assembly tools such as GetOrganelle and MITObim assume that input reads are largely free of such artifacts (Hahn et al., 2013; Jin et al., 2020). Consequently, undetected chimeras may produce fragmented assemblies or misidentified organellar boundaries. To ensure accurate reconstruction of mitochondrial genomes, a reliable method for detecting and filtering PCR-induced chimeras before assembly is essential.

This study focuses on mitochondrial sequencing data from the genus *Sardinella*, a group of small pelagic fishes widely distributed in Philippine waters. Among them, *Sardinella lemuru* (Bali sardinella) is one of the country's most abundant and economically important species, providing protein and livelihood to coastal communities (Labrador, Agmata, Palermo, Ravago-Gotanco, & Pante, 2021; Willette, Bognot, Mutia, & Santos, 2011). Accurate mitochondrial assemblies are critical for understanding its population genetics, stock structure, and evolutionary history. However, assembly pipelines often encounter errors or fail to complete due to undetected chimeric reads. To address this gap, this research introduces MitoChime, a machine learning pipeline designed to detect and filter PCR-induced chimeric reads using both alignment-based and sequence-derived statistical features. The tool aims to provide bioinformatics laboratories, partic-

151 ularly the Philippine Genome Center Visayas (PGC Visayas), with an efficient
152 solution for improving mitochondrial genome reconstruction.

153 1.2 Problem Statement

154 While NGS technologies have revolutionized genomic data acquisition, the ac-
155 curacy of mitochondrial genome assembly remains limited by artifacts produced
156 during PCR amplification. These chimeric reads can distort assembly graphs and
157 cause misassemblies, with particularly severe effects in small, circular mitochon-
158 drial genomes (Boore, 1999; Cameron, 2014). Existing assembly pipelines such
159 as GetOrganelle, MITObim, and NOVOPlasty assume that sequencing reads are
160 free of such artifacts (Dierckxsens et al., 2017; Hahn et al., 2013; Jin et al., 2020).
161 At PGC Visayas, several mitochondrial assemblies have failed or yielded incom-
162 plete contigs despite sufficient coverage, suggesting that undetected chimeric reads
163 compromise assembly reliability. Meanwhile, existing chimera detection tools such
164 as UCHIME and VSEARCH were developed primarily for amplicon-based com-
165 munity analysis and rely heavily on reference or taxonomic comparisons (Edgar,
166 Haas, Clemente, Quince, & Knight, 2011; Rognes, Flouri, Nichols, Quince, &
167 Mahé, 2016). These approaches are unsuitable for single-species organellar data,
168 where complete reference genomes are often unavailable. Therefore, there is a
169 pressing need for a reference-independent, data-driven tool capable of detecting
170 and filtering PCR-induced chimeras in mitochondrial sequencing datasets.

¹⁷¹ 1.3 Research Objectives

¹⁷² 1.3.1 General Objective

¹⁷³ This study aims to develop and evaluate a machine learning-based pipeline (Mi-
¹⁷⁴ toChime) that detects PCR-induced chimeric reads in *Sardinella lemuru* mito-
¹⁷⁵ chondrial sequencing data in order to improve the quality and reliability of down-
¹⁷⁶ stream mitochondrial genome assemblies.

¹⁷⁷ 1.3.2 Specific Objectives

¹⁷⁸ Specifically, the study aims to:

- ¹⁷⁹ 1. construct simulated *Sardinella lemuru* Illumina paired-end datasets contain-
¹⁸⁰ ing both clean and PCR-induced chimeric reads,
- ¹⁸¹ 2. extract alignment-based and sequence-based features such as k-mer compo-
¹⁸² sition, junction complexity, and split-alignment counts from both clean and
¹⁸³ chimeric reads,
- ¹⁸⁴ 3. train, validate, and compare supervised machine learning models for classi-
¹⁸⁵ fying reads as clean or chimeric,
- ¹⁸⁶ 4. determine feature importance and identify indicators of PCR-induced
¹⁸⁷ chimerism,
- ¹⁸⁸ 5. integrate the optimized classifier into a modular and interpretable pipeline
¹⁸⁹ deployable on standard computing environments at PGC Visayas.

190 **1.4 Scope and Limitations of the Research**

191 This study focuses on detecting PCR-induced chimeric reads in Illumina paired-
192 end mitochondrial sequencing data from *Sardinella lemuru*. The decision to re-
193 strict the taxonomic scope to a single species is based on four considerations: to
194 limit interspecific variation in mitochondrial genome size, GC content, and repeti-
195 tive regions so that differences in read patterns can be attributed more directly to
196 PCR-induced chimerism; to align the analysis with relevant *S. lemuru* sequencing
197 projects at PGC Visayas; to take advantage of the availability of *S. lemuru* mito-
198 chondrial assemblies and raw datasets in public repositories such as the National
199 Center for Biotechnology Information (NCBI), which facilitates reference selection
200 and benchmarking; and to develop a tool that directly supports local studies on
201 *S. lemuru* population structure and fisheries management.

202 The study emphasizes `wgsim`-based simulations and selected empirical mito-
203 chondrial datasets from *S. lemuru*. It excludes naturally occurring chimeras, nu-
204 clear mitochondrial pseudogenes (NUMTs), and large-scale assembly rearrange-
205 ments in nuclear genomes. Feature extraction is restricted to low-dimensional
206 alignment and sequence statistics, such as k-mer frequency profiles, GC content,
207 read length, soft and hard clipping metrics, split-alignment counts, and map-
208 ping quality, rather than high-dimensional deep learning embeddings. This de-
209 sign keeps model behaviour interpretable and ensures that the pipeline can be
210 run on standard workstations at PGC Visayas. Testing on long-read platforms
211 (e.g., Nanopore, PacBio) and other taxa is outside the scope of this project; the
212 implemented pipeline is evaluated only on short-read *S. lemuru* datasets.

213 Other limitations in this study include the following: simulations with varying

214 error rates were not performed, so the effect of different sequencing errors on model
215 performance remains unexplored; alternative parameter settings, including k-mer
216 lengths and microhomology window sizes, were not systematically tested, which
217 could affect the sensitivity of both k-mer and microhomology feature detection as
218 well as the identification of chimeric junctions; and the machine learning models
219 rely on supervised training with labeled examples, which may limit their ability
220 to detect novel or unexpected chimeric patterns.

221 1.5 Significance of the Research

222 This research provides both methodological and practical contributions to mito-
223 chondrial genomics and bioinformatics. First, MitoChime detects PCR-induced
224 chimeric reads prior to genome assembly, with the goal of improving the con-
225 tinuity and correctness of *Sardinella lemuru* mitochondrial assemblies. Second,
226 it replaces informal manual curation with a documented workflow, improving au-
227 tomation and reproducibility. Third, the pipeline is designed to run on computing
228 infrastructures commonly available in regional laboratories, enabling routine use
229 at facilities such as PGC Visayas. Finally, more reliable mitochondrial assemblies
230 for *S. lemuru* provide a stronger basis for downstream applications in the field of
231 fisheries and genomics.

²³² **Chapter 2**

²³³ **Review of Related Literature**

²³⁴ This chapter presents an overview of the literature relevant to the study. It
²³⁵ discusses the biological and computational foundations underlying mitochondrial
²³⁶ genome analysis and assembly, as well as existing tools, algorithms, and techniques
²³⁷ related to chimera detection and genome quality assessment. The chapter aims to
²³⁸ highlight the strengths, limitations, and research gaps in current approaches that
²³⁹ motivate the development of the present study.

²⁴⁰ **2.1 The Mitochondrial Genome**

²⁴¹ Mitochondrial genome (mtDNA) is a small, typically circular molecule found in
²⁴² most eukaryotes. It encodes essential genes involved in oxidative phosphorylation
²⁴³ and energy metabolism. Because of its conserved structure, mtDNA has become
²⁴⁴ a valuable genetic marker for studies in population genetics and phylogenetics
²⁴⁵ (Anderson et al., 1981; Boore, 1999). In animal species, the mitochondrial genome

246 ranges from 15–20 kilobase and contains 13 protein-coding genes, 22 tRNAs, and
247 two rRNAs arranged compactly without introns (Gray, 2012). In comparison to
248 nuclear DNA, the ratio of the number of copies of mtDNA is higher and has
249 simple organization which make it particularly suitable for genome sequencing
250 and assembly studies (Dierckxsens et al., 2017).

251 **2.1.1 Mitochondrial Genome Assembly**

252 Mitochondrial genome assembly refers to the reconstruction of the complete mito-
253 chondrial DNA (mtDNA) sequence from raw or fragmented sequencing reads. It is
254 conducted to obtain high-quality, continuous representations of the mitochondrial
255 genome that can be used for a wide range of analyses, including species identi-
256 fication, phylogenetic reconstruction, evolutionary studies, and investigations of
257 mitochondrial diseases. Because mtDNA evolves rapidly, its assembled sequence
258 provides valuable insights into population structure, lineage divergence, and adap-
259 tive evolution across taxa (Boore, 1999). Compared to nuclear genome assembly,
260 assembling the mitochondrial genome is often considered more straightforward but
261 still encounters technical challenges such as the formation of chimeric reads. Com-
262 monly used tools for mitogenome assembly such as GetOrganelle and MITObim
263 operate under the assumption of organelle genome circularity, and are vulnerable
264 when chimeric reads disrupt this circular structure, resulting in assembly errors
265 (Hahn et al., 2013; Jin et al., 2020).

266 2.2 PCR Amplification and Chimera Formation

267 PCR plays an important role in NGS library preparation, as it amplifies target
268 DNA fragments for downstream analysis. However as previously mentioned, the
269 amplification process can also introduce chimeric reads which compromises the
270 quality of the input reads supplied to sequencing or assembly workflows. Chimeras
271 typically arise when incomplete extension occurs during a PCR cycle. This causes
272 the DNA polymerase to switch from one template to another and generate hy-
273 brid recombinant molecules (Judo et al., 1998). Artificial chimeras are produced
274 through such amplification errors, whereas biological chimeras occur naturally
275 through genomic rearrangements or transcriptional events.

276 In the context of amplicon-based sequencing, the presence of chimeras can in-
277 flate estimates of genetic or microbial diversity and may cause misassemblies dur-
278 ing genome reconstruction. Qin et al. (2023) has reported that chimeric sequences
279 may account for more than 10% of raw reads in amplicon datasets. This artifact
280 tends to be most prominent among rare operational taxonomic units (OTUs) or
281 singletons, which are sometimes misinterpreted as novel diversity, further caus-
282 ing the complication of microbial diversity analyses (Gonzalez, Zimmermann, &
283 Saiz-Jimenez, 2004). As such, determining and minimizing PCR-induced chimera
284 formation is vital for improving the quality of mitochondrial genome assemblies,
285 and ensuring the reliability of amplicon sequencing data.

286 **2.3 Existing Traditional Approaches for Chimera**

287 **Detection**

288 Several computational tools have been developed to identify chimeric sequences in
289 NGS datasets. These tools generally fall into two categories: reference-based and
290 de novo approaches. Reference-based chimera detection, also known as database-
291 dependent detection, is one of the earliest and most widely used computational
292 strategies for identifying chimeric sequences in amplicon-based community studies.
293 These methods rely on the comparison of each query sequence against a curated,
294 high-quality database of known, non-chimeric reference sequences (Edgar et al.,
295 2011).

296 On the other hand, the de novo chimera detection, also referred to as reference-
297 free detection, represents an alternative computational paradigm that identifies
298 chimeric sequences without reliance on external reference databases. This method
299 infer chimeras based on internal relationships among the sequences present within
300 the dataset itself, making it particularly advantageous in studies of under explored
301 or taxonomically diverse communities where comprehensive reference databases
302 are unavailable or incomplete (Edgar, 2016; Edgar et al., 2011). The underlying
303 assumption on this method is that during PCR, true biological sequences are
304 generally more abundant as they are amplified early and dominate the read pool,
305 whereas chimeric sequences appear later and are generally less abundant. The
306 de novo approach leverage this abundance hierarchy, treating the most abundant
307 sequences as supposed parents and testing whether less abundant sequences can
308 be reconstructed as mosaics of these templates. Compositional and structural
309 similarity are also evaluated to check whether different regions of a candidate

310 sequence correspond to distinct high-abundance sequences.

311 In practice, many modern bioinformatics pipelines combine both paradigms
312 sequentially: an initial de novo step identifies dataset-specific chimeras, followed
313 by a reference-based pass that removes remaining artifacts relative to established
314 databases (Edgar, 2016). These two methods of detection form the foundation of
315 tools such as UCHIME and later UCHIME2.

316 2.3.1 UCHIME

317 UCHIME is one of the most widely used tools for detecting chimeric sequences in
318 amplicon-based studies and remains a standard quality-control step in microbial
319 community analysis. Its core strategy is to test whether a query sequence (Q) can
320 be explained as a mosaic of two parent sequences, (A and B), and to score this
321 relationship using a structured alignment model (Edgar et al., 2011).

322 In reference mode, UCHIME divides the query into several segments and maps
323 them against a curated database of non-chimeric sequences. Candidate parents
324 are identified, and a three-way alignment is constructed. The algorithm assigns
325 “Yes” votes when different segments of the query match different parents and
326 “No” votes when the alignment contradicts a chimeric pattern. The final score
327 reflects the balance of these votes. In de novo mode, UCHIME operationalizes the
328 abundance-skew principle described earlier: high-abundance sequences are treated
329 as candidate parents, and lower-abundance sequences are evaluated as potential
330 mosaics. This makes the method especially useful when no reliable reference
331 database exists.

332 Although UCHIME is highly sensitive, it faces key constraints. Chimeras
333 formed from parents with very low divergence (below 0.8%) are difficult to detect
334 because they are nearly indistinguishable from sequencing errors. Accuracy in ref-
335 erence mode depends strongly on database completeness, while de novo detection
336 assumes that true parents are both present and sufficiently more abundant, such
337 conditions are not always met.

338 **2.3.2 UCHIME2**

339 UCHIME2 extends the original algorithm with refinements tailored for high-
340 resolution sequencing data. One of its major contributions is a re-evaluation
341 of benchmarking practices. Edgar (2016) demonstrated that earlier accuracy es-
342 timates for chimera detection were overly optimistic because they relied on un-
343 realistic scenarios where all true parent sequences were assumed to be present.
344 Using the more rigorous CHSIMA benchmark, UCHIME2 showed the prevalence
345 of “fake models” or real biological sequences that can be perfectly reconstructed
346 as apparent chimeras of other sequences, which suggests that perfect chimera de-
347 tection is theoretically unattainable. UCHIME2 also introduces several preset
348 modes (e.g., denoised, balanced, sensitive, specific, high-confidence) designed to
349 tune sensitivity and specificity depending on dataset characteristics. These modes
350 allow users to adjust the algorithm to the expected noise level or analytical goals.

351 Despite these improvements, UCHIME2 must be applied with caution. The
352 author’s website manual (Edgar, n.d) explicitly advises against using UCHIME2
353 as a standalone chimera-filtering step in OTU clustering or denoising workflows
354 because doing so can inflate both false positives and false negatives.

355 2.3.3 CATch

356 As previously mentioned, UCHIME (Edgar et al., 2011) relied on alignment-based
357 sequences in amplicon data. However, researchers soon observed that different al-
358 gorithms often produced inconsistent predictions. A sequence might be identified
359 as chimeric by one tool but classified as non-chimeric by another, resulting in
360 unreliable filtering outcomes across studies.

361 To address these inconsistencies, Mysara, Saeys, Leys, Raes, and Monsieurs
362 (2015) developed the Classifier for Amplicon Tool Chimeras (CATCh), which rep-
363 resents the first ensemble machine learning system designed for chimera detection
364 in 16S rRNA amplicon sequencing. Rather than depending on a single detec-
365 tion strategy, CATCh integrates the outputs of several established tools, includ-
366 ing UCHIME, ChimeraSlayer, DECIPHER, Pintail, and Perseus. The individual
367 scores and binary decisions generated by these tools are used as input features for
368 a supervised learning model. The algorithm employs a Support Vector Machine
369 (SVM) with a Pearson VII Universal Kernel (PUK) to determine optimal weight-
370 ings among the input features and to assign each sequence a probability of being
371 chimeric.

372 Benchmarking in both reference-based and de novo modes demonstrated signif-
373 icant performance improvements. CATCh achieved sensitivities of approximately
374 85 percent in reference-based mode and 92 percent in de novo mode, with corre-
375 sponding specificities of approximately 96 percent and 95 percent. These results
376 indicate that CATCh detected 7 to 12 percent more chimeras than any individual
377 algorithm while maintaining high precision.

378 2.3.4 ChimPipe

379 Among the available tools for chimera detection, ChimPipe is a pipeline developed
380 to identify chimeric sequences such as biological chimeras. It uses both discordant
381 paired-end reads and split-read alignments to improve the accuracy and sensitivity
382 of detecting biological chimeras (Rodriguez-Martin et al., 2017). By combining
383 these two sources of information, ChimPipe achieves better precision than meth-
384 ods that depend on a single type of indicator.

385 The pipeline works with many eukaryotic species that have available genome
386 and annotation data (Rodriguez-Martin et al., 2017). It can also predict multiple
387 isoforms for each gene pair and identify breakpoint coordinates that are useful
388 for reconstructing and verifying chimeric transcripts. Tests using both simulated
389 and real datasets have shown that ChimPipe maintains high accuracy and reliable
390 performance.

391 ChimPipe lets users adjust parameters to fit different sequencing protocols or
392 organism characteristics. Experimental results have confirmed that many chimeric
393 transcripts detected by the tool correspond to functional fusion proteins, demon-
394 strating its utility for understanding chimera biology and its potential applications
395 in disease research (Rodriguez-Martin et al., 2017).

396 **2.4 Machine Learning Approaches for Chimera**

397 **and Sequence Quality Detection**

398 Traditional chimera detection tools rely primarily on heuristic or alignment-based
399 rules. Recent advances in machine learning (ML) have demonstrated that models
400 trained on sequence-derived features can effectively capture compositional and
401 structural patterns in biological sequences. Although most existing ML systems
402 such as those used for antibiotic resistance prediction, taxonomic classification,
403 or viral identification are not specifically designed for chimera detection, they
404 highlight how data-driven models can outperform similarity-based heuristics by
405 learning intrinsic sequence signatures. In principle, ML frameworks can integrate
406 indicators such as k-mer frequencies, GC-content variation and split-alignment
407 metrics to identify subtle anomalies that may indicate a chimeric origin (Arango
408 et al., 2018; Liang, Bible, Liu, Zou, & Wei, 2020; Ren et al., 2020).

409 **2.4.1 Feature-Based Representations of Genomic Se-**

410 **quences**

411 Feature extraction converts DNA sequences into numerical representations suit-
412 able for machine learning models. One approach is k-mer frequency analysis,
413 which counts short nucleotide sequences within a read (Vervier, Mahé, Tournoud,
414 Veyrieras, & Vert, 2015). High-frequency k-mers, including simple repeats such
415 as “AAAAAA,” can highlight repetitive or unusual regions that may occur near
416 chimeric junctions. Comparing k-mer patterns across adjacent parts of a read can
417 help identify such regions, while GC content provides an additional descriptor of

418 local sequence composition (Ren et al., 2020).

419 Alignment-derived features further inform junction detection. Long-read tools
420 such as Sniffles (Sedlazeck et al., 2018) use split alignments to locate breakpoints
421 across extended sequences, whereas short-read aligners like Minimap2 (Li, 2018)
422 report supplementary and secondary alignments that indicate local discontinu-
423 ities. Split alignments, where parts of a read map to different regions, can reveal
424 template-switching events. These features complement k-mer profiles and en-
425 hance detection of potentially chimeric reads, even in datasets with incomplete
426 references.

427 Microhomology, or short sequences shared between adjacent segments, is an-
428 other biologically meaningful feature. Short microhomologies, typically 3–20 bp,
429 are involved in template switching both in cellular repair pathways and during
430 PCR, where they act as signatures of chimera formation (Peccoud et al., 2018;
431 Sfeir & Symington, 2015). In PCR-induced chimeras, short identical sequences
432 at junctions provide a clear signature of chimerism. Measuring the longest exact
433 overlap at each breakpoint complements k-mer and alignment features and helps
434 identify reads that are potentially chimeric.

435 2.5 Synthesis of Chimera Detection Approaches

436 To provide an integrated overview of the literature discussed in this chapter, Ta-
437 ble 2.1 summarizes the major chimera detection studies, their methodological
438 approaches, and their known limitations.

Table 2.1: Comparison of Chimera Detection Approaches and Tools

Method / Tool	Core Approach	Key Limitations
Reference-based Detection	Compares each query sequence against curated databases of verified, non-chimeric sequences; evaluates segment similarity to identify mosaic patterns.	Accuracy depends on database completeness; performs poorly for novel taxa or missing parents; limited sensitivity for low-divergence chimeras.
De novo Detection	Identifies chimeras using only internal dataset structure; leverages abundance hierarchy and compositional similarity to infer whether low-abundance sequences can be reconstructed from abundant parents.	Assumes true sequences are more abundant; fails when amplification bias distorts abundances; struggles when parental sequences are similarly abundant or highly similar.
UCHIME	Alignment-based model that partitions the query into segments, identifies parent candidates, and computes a chimera score via a three-way alignment; supports reference and de novo modes.	Reduced accuracy for very closely related parents (<0.8% divergence); sensitive to incomplete databases; de novo mode fails if parents are absent or not sufficiently more abundant.
UCHIME2	Updated UCHIME with improved benchmarking (CHSIMA) and multiple sensitivity/specificity presets; better handles incomplete references and dataset variability.	“Fake models” limit theoretical accuracy; genuine variants may mimic chimeras; not recommended as a standalone step in OTU or denoising pipelines due to increased false positives/negatives.
CATCh	First ensemble ML model for 16S chimera detection; integrates outputs of UCHIME, ChimeraSlayer, DECIPHER, Pintail, and Perseus using an SVM to boost overall prediction accuracy.	Performance constrained by underlying tools; ML model cannot capture features not present in component algorithms; may misclassify in highly novel or low-coverage datasets.
ChimPipe	Pipeline for detecting biological chimeras in RNA-seq using discordant paired-end reads and split-read alignments; identifies isoforms and breakpoint coordinates.	Requires high-quality genome and annotation; tailored to RNA-seq rather than amplicons; computationally intensive; limited to organisms with available reference genomes.

439 Across existing studies, no single approach reliably detects all forms of chimeric
440 sequences, and the reviewed literature consistently shows that chimeras remain a
441 persistent challenge in genomics and bioinformatics. Although the surveyed tools
442 are not designed specifically for organelle genome assembly, they provide valua-
443 ble insights into which methodological strategies are effective and where current
444 approaches fall short. These limitations collectively define a clear research gap:
445 the need for a specialized, feature-driven detection framework tailored to PCR-
446 induced mitochondrial chimeras. Addressing this gap aligns with the research
447 objective outlined in Section 1.3, which is to develop and evaluate a machine
448 learning-based pipeline (MitoChime) that improves the quality of downstream
449 mitochondrial genome assembly. In support of this aim, the subsequent chapters
450 describe the design, implementation, and evaluation of the proposed tool.

⁴⁵¹ Chapter 3

⁴⁵² Research Methodology

⁴⁵³ This chapter outlines the steps involved in completing the study, including data
⁴⁵⁴ gathering, generating simulated mitochondrial Illumina reads, preprocessing and
⁴⁵⁵ indexing the data, developing a feature extraction pipeline to extract key features,
⁴⁵⁶ applying machine learning algorithms for chimera detection, and validating and
⁴⁵⁷ comparing model performance.

⁴⁵⁸ 3.1 Research Activities

⁴⁵⁹ As illustrated in Figure 3.1, this study carried out a sequence of procedures to
⁴⁶⁰ detect PCR-induced chimeric reads in mitochondrial genomes. The process began
⁴⁶¹ with collecting a mitochondrial reference sequence of *Sardinella lemuru* from the
⁴⁶² National Center for Biotechnology Information (NCBI) database, which was used
⁴⁶³ as a reference for generating simulated clean and chimeric reads. These reads
⁴⁶⁴ were subsequently indexed and mapped. The resulting collections then passed

465 through a feature extraction pipeline that extracted k-mer profiles, supplementary
466 alignment (SA) features, and microhomology information to prepare the data for
467 model construction. The machine learning model was trained using the processed
468 input, and its precision and accuracy were assessed. It underwent tuning until it
469 reached the desired performance threshold, after which it proceeded to validation
470 and will undergo external testing.

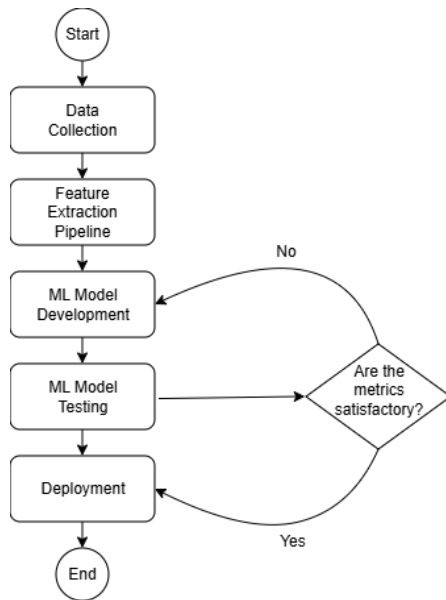


Figure 3.1: Process Diagram of Special Project

471 3.1.1 Data Collection

472 The mitochondrial genome reference sequence of *S. lemuru* was obtained from the
473 NCBI database (accession number NC_039553.1) in FASTA format and was used
474 to generate simulated reads.

475 This step was scheduled to begin in the first week of November 2025 and
476 expected to be completed by the end of that week, with a total duration of ap-

477 proximately one (1) week.

478 **Data Preprocessing**

479 All steps in the simulation and preprocessing pipeline were executed using a cus-
480 tom script in Python (Version 3.11). The script runs each stage, including read
481 simulation, reference indexing, mapping, and alignment processing, in a fixed se-
482 quence.

483 `wgsim` (Version 1.13) was used to simulate 10,000 paired-end fragments, pro-
484 ducing 20,000 reads (10,000 forward and 10,000 reverse) from the original refer-
485 ence (`original_reference.fasta`) and designated as clean reads. The tool was
486 selected because it provides fast generation of Illumina-like reads with controllable
487 error rates, using the following command:

```
488 wgsim -1 150 -2 150 -r 0 -R 0 -X 0 -e 0.001 -N 10000 \
489     original_reference.fasta ref1.fastq ref2.fastq
```

490 Chimeric sequences were then generated from the same reference FASTA
491 file using a separate Python script. Two non-adjacent segments were randomly
492 selected such that their midpoint distances fell within specified minimum and
493 maximum thresholds. The script attempts to retain microhomology to mimic
494 PCR-induced template switching. The resulting chimeras were written to
495 `chimera_reference.fasta` and was processed with `wgsim` to simulate 10,000
496 paired-end fragments, generating 20,000 chimeric reads (10,000 forward reads in
497 `chimeric1.fastq` and 10,000 reverse reads in `chimeric2.fastq`) using the same
498 command format above.

499 Next, a `minimap2` index of the reference genome was created using:

```
500  minimap2 -d ref.mmi original_reference.fasta
```

501 Minimap2 (Version 2.28) was used to map simulated clean and chimeric reads
502 to the original reference. An index (`ref.mmi`) was first generated to enable efficient
503 alignment, and mapping produced the alignment features used as input for the
504 machine learning model. The reads were mapped using the following command:

```
505  minimap2 -ax sr -t 8 ref.mmi ref1.fastq ref2.fastq > clean.sam
```

```
506  minimap2 -ax sr -t 8 ref.mmi \  
507  chimeric1.fastq chimeric2.fastq > chimeric.sam
```

508 The resulting clean and chimeric SAM files contain the alignment positions of
509 each read relative to the original reference genome. These files were then converted
510 to BAM format, sorted, and indexed using `samtools` (Version 1.20):

```
511  samtools view -bS clean.sam -o clean.bam  
512  samtools view -bS chimeric.sam -o chimeric.bam  
513  
514  samtools sort clean.bam -o clean.sorted.bam  
515  samtools index clean.sorted.bam  
516  
517  samtools sort chimeric.bam -o chimeric.sorted.bam  
518  samtools index chimeric.sorted.bam
```

519 The total number of simulated reads was expected to be 40,000. The final col-
520 lection of reads contained 19,984 clean reads and 20,000 chimeric reads (39,984 en-
521 tries in total), providing a roughly balanced distribution between the two classes.
522 After alignment with `minimap2`, only 19,984 clean reads remained because un-
523 mapped reads were not included in the BAM file. Some sequences failed to align
524 due to the 5% error rate defined during `wgsim` simulation, which produced mis-
525 matches that caused certain reads to fall below the aligner's matching threshold.

526 This whole process was scheduled to start in the second week of November 2025
527 and was expected to be completed by the last week of November 2025, with a total
528 duration of approximately three (3) weeks.

529 **3.1.2 Feature Extraction Pipeline**

530 This stage directly follows the previous alignment phase, utilizing the resulting
531 BAM files (specifically `chimeric.sorted.bam` and `clean.sorted.bam`). A cus-
532 tom Python script was created to efficiently process each primary-mapped read
533 to extract the necessary set of features, which are then compiled into a structured
534 feature matrix in TSV format. The pipeline's core functionality relies on libraries,
535 namely `Pysam` (Version 0.22) for the robust parsing of BAM structures and `NumPy`
536 (Version 1.26) for array operations and computations. To ensure correctness and
537 adherence to best practices, bioinformatics experts at the PGC Visayas will be
538 consulted to validate the pipeline design, feature extraction logic, and overall data
539 integrity.

540 This stage of the study was scheduled to begin in the last week of November

541 2025 and conclude by the first week of December 2025, with an estimated total
542 duration of approximately two (2) weeks.

543 The pipeline focuses on three features that collectively capture biological sig-
544 natures associated with PCR-induced chimeras: (1) supplementary alignment flag
545 (SA), (2) k-mer composition difference, and (3) microhomology.

546 **Supplementary Alignment Flag**

547 Split-alignment information was derived from the SA tag embedded in each pri-
548 mary read of the BAM file. This tag is typically associated with reads that map to
549 multiple genomic locations, suggesting a chimeric structure. To extract this infor-
550 mation, the script first checked whether the read carried an SA:Z tag. If present,
551 the tag string was parsed using the function `parse_sa_tag`, yielding metadata for
552 each alignment containing the reference name, mapped position, strand, mapping
553 quality, and number of mismatches.

554 After parsing, the function `sa_feature_stats` was applied to establish the fun-
555 damental split indicators, `has_sa` and `sa_count`. Along with these initial counts,
556 the function aggregated the metrics related to the structure and reliability of the
557 split alignments.

558 **K-mer Composition Difference**

559 Comparing k-mer frequency profiles between the left and right halves of a read
560 allows for the detection of abrupt compositional shifts, independent of alignment
561 information.

562 The script implemented this by inferring a likely junction breakpoint using the
563 function `infer_breakpoints`, prioritizing the boundaries defined by soft-clipping
564 operations. If no clipping was present, the midpoint of the alignment or the read
565 length was utilized as a fallback. The read sequence was then divided into left and
566 right segments at this inferred breakpoint, and k-mer frequency profiles ($k = 6$)
567 were generated for both halves, ignoring any k-mers containing ambiguous 'N'
568 bases. The resulting k-mer frequency vectors are then normalized and compared
569 using the functions `cosine_difference` and `js_divergence`.

570 **Microhomology**

571 The process of extracting the microhomology feature started by utilizing the func-
572 tion `infer_breakpoints` similar to the k-mer workflow. Once a breakpoint was es-
573 tablished, the script scanned a ± 40 base pair window surrounding the breakpoint
574 and used the function `longest_suffix_prefix_overlap` to identify the longest
575 exact suffix-prefix overlap between the left and right read segments. This overlap,
576 which represents consecutive bases shared at the junction, was recorded as the
577 `microhomology_length` in the dataset. The 40-base pair window was chosen to
578 ensure that short shared sequences at or near the breakpoint were captured, with-
579 out including distant sequences that are unrelated. Additionally, the GC content
580 of the overlapping sequence was calculated using the function `gc_content`, which
581 counts guanine (G) and cytosine (C) bases within the detected microhomology
582 and divides by the total length, yielding a proportion between 0 and 1, and was
583 stored under the `microhomology_gc` attribute. Microhomology was quantified
584 using a (3–20) bp window, consistent with values reported in prior research on
585 PCR-induced chimeras. Moreover, a k-mer length of 6 was used to capture pat-

586 terns within the 40-bp window surrounding each breakpoint. This length is long
587 enough to detect informative sequence shifts at junctions.

588 3.1.3 Machine Learning Model Development

589 After feature extraction, the per-read feature matrices for clean and chimeric
590 reads were merged into a single dataset. Each row corresponded to one paired-
591 end read, and columns encoded alignment-structure features (e.g., supplementary
592 alignment count and spacing between segments), CIGAR-derived soft-clipping
593 statistics (e.g., left and right soft-clipped length, total clipped bases), k-mer com-
594 position discontinuity between read segments, and microhomology descriptors
595 near candidate junctions. The resulting feature set was restricted to quantities
596 that can be computed from standard BAM/FASTQ files in typical mitochondrial
597 sequencing workflows.

598 The labelled dataset was randomly partitioned into training (80%) and test
599 (20%) subsets using stratified sampling to preserve the 1:1 ratio of clean to
600 chimeric reads. Model development and evaluation were implemented in Python
601 (Version 3.11) using the `scikit-learn`, `xgboost`, `lightgbm`, and `catboost`
602 libraries. A broad panel of classification algorithms was then benchmarked on the
603 training data to obtain a fair comparison of different model families under identical
604 feature conditions. The panel included: a trivial dummy classifier, L_2 -regularized
605 logistic regression, a calibrated linear support vector machine (SVM), k -nearest
606 neighbours, Gaussian Naïve Bayes, decision-tree ensembles (Random Forest, Ex-
607 tremely Randomized Trees, and Bagging with decision trees), gradient boosting
608 methods (Gradient Boosting, XGBoost, LightGBM, and CatBoost), and a shallow

609 multilayer perceptron (MLP).

610 For each model, five-fold stratified cross-validation was performed on the training
611 set. In every fold, four-fifths of the data were used for fitting and the remaining
612 one-fifth for validation. Mean cross-validation accuracy, precision, recall, F1-score
613 for the chimeric class, and area under the receiver operating characteristic curve
614 (ROC–AUC) were computed to summarize performance and rank candidate methods.
615 This baseline screen allowed comparison of linear, probabilistic, neural, and
616 ensemble-based approaches and identified tree-based ensemble and boosting models
617 as consistently strong performers relative to simpler baselines.

618 3.1.4 Model Benchmarking, Hyperparameter Optimization, 619 and Evaluation

620 Model selection and refinement proceeded in two stages. First, the cross-validation
621 results from the broad panel were used to identify a subset of competitive models
622 for more detailed optimization. Specifically, ten model families were carried
623 forward: L_2 -regularized logistic regression, calibrated linear SVM, Random Forest,
624 ExtraTrees, Gradient Boosting, XGBoost, LightGBM, CatBoost, Bagging
625 with decision trees, and a shallow MLP. This subset spans both linear and non-
626 linear decision boundaries, but emphasizes ensemble and boosting methods, which
627 showed superior F1 and ROC–AUC in the initial benchmark.

628 Second, hyperparameter optimization was conducted for each of the ten selected
629 models using randomized search with five-fold stratified cross-validation
630 (`RandomizedSearchCV`). For tree-based ensembles, the search space included the

631 number of trees, maximum depth, minimum samples per split and leaf, and the
632 fraction of features considered at each split. For boosting methods, key hyper-
633 parameters such as the number of boosting iterations, learning rate, tree depth,
634 subsampling rate, and column subsampling rate were tuned. For the MLP, the
635 number and size of hidden layers, learning rate, and L_2 -regularization strength
636 were varied. In all cases, the primary optimisation criterion was the F1-score of
637 the chimeric class, averaged across folds.

638 For each model family, the hyperparameter configuration with the highest
639 mean cross-validation F1-score was selected as the best-tuned estimator. These
640 tuned models were then refitted on the full training set and evaluated once on the
641 held-out test set to obtain unbiased estimates of performance. Test-set metrics in-
642 cluded accuracy, precision, recall, F1-score for the chimeric class, and ROC–AUC.
643 Confusion matrices and ROC curves were generated for the top-performing mod-
644 els to characterise common error modes, such as false negatives (missed chimeric
645 reads) and false positives (clean reads incorrectly labelled as chimeric). The final
646 model or small set of models for downstream interpretation was chosen based on
647 a combination of test-set F1-score, and ROC–AUC.

648 3.1.5 Feature Importance and Interpretation

649 To relate model decisions to biologically meaningful signals, feature-importance
650 analyses were performed on the best-performing tree-based models. Two comple-
651 mentary approaches were used. First, built-in importance measures from ensemble
652 methods (e.g., split-based importances in Random Forest and Gradient Boosting)
653 were examined to obtain an initial ranking of features based on their contribution

654 to reducing impurity. Second, model-agnostic permutation importance was com-
655 puted on the test set by repeatedly permuting each feature column while keeping
656 all others fixed and measuring the resulting decrease in F1-score. Features whose
657 permutation led to a larger performance drop were interpreted as more influential
658 for chimera detection.

659 For interpretability, individual features were grouped into four conceptual
660 families: (i) supplementary alignment and alignment-structure features (e.g., SA
661 count, spacing between alignment segments, strand consistency), (ii) soft-clipping
662 features (e.g., left and right soft-clipped length, total clipped bases), (iii) k-mer
663 composition discontinuity features (e.g., cosine distance and Jensen–Shannon di-
664 vergence between k-mer profiles of read segments), and (iv) microhomology de-
665 scriptors (e.g., microhomology length and local GC content around putative break-
666 points). This analysis provided a basis for interpreting the trained models in
667 terms of known mechanisms of PCR-induced template switching and for identi-
668 fying which alignment-based and sequence-derived cues are most informative for
669 distinguishing chimeric from clean mitochondrial reads.

670 **3.1.6 Validation and Testing**

671 Validation will involve both internal and external evaluations. Internal validation
672 was achieved through five-fold cross-validation on the training data to verify model
673 generalization and reduce variance due to random sampling. External testing was
674 performed on the 20% hold-out dataset from the simulated reads, providing an un-
675 biased assessment of model generalization. Feature extraction and preprocessing
676 were applied consistently across all splits.

677 Comparative evaluation was performed across all candidate algorithms to de-
678 termine which models demonstrated the highest predictive performance and com-
679 putational efficiency under identical data conditions. Their metrics were compared
680 to identify which algorithms were most suitable for further refinement.

681 3.1.7 Documentation

682 Comprehensive documentation was maintained throughout the study to ensure
683 transparency and reproducibility. All stages of the research, including data gath-
684 ering, preprocessing, feature extraction, model training, and validation, were sys-
685 tematically recorded in a `.README` file in the GitHub repository. For each ana-
686 lytical step, the corresponding parameters, software versions, and command line
687 scripts were documented to enable exact replication of results.

688 The repository structure followed standard research data management prac-
689 tices, with clear directories for datasets and scripts. Computational environments
690 were standardized using Conda, with an environment file (`environment.yml`)
691 specifying dependencies and package versions to maintain consistency across sys-
692 tems.

693 For manuscript preparation and supplementary materials, Overleaf (L^AT_EX)
694 was used to produce publication-quality formatting and consistent referencing.

695 3.2 Calendar of Activities

696 Table 3.1 presents the project timeline in the form of a Gantt chart, where each
697 bullet point corresponds to approximately one week of planned activity.

Table 3.1: Timetable of Activities

Activities (2025)	Nov	Dec	Jan	Feb	Mar	Apr	May
Data Collection and Simulation	• • •						
Feature Extraction Pipeline	•	•					
Machine Learning Development		•	••	• • •	• • •	••	
Testing and Validation						••	• • •
Documentation	• • •	• • •	• • •	• • •	• • •	• • •	• • •

698 Chapter 4

699 Results and Discussion

700 4.1 Descriptive Analysis of Features

701 This chapter presents the performance of the proposed feature set and machine
702 learning models for detecting PCR-induced chimeric reads in simulated mitochon-
703 drial Illumina data. The behaviour of the main features is first described, followed
704 by a comparison of baseline classifiers, an assessment of the effect of hyperparam-
705 eter tuning, and an analysis of feature importance in terms of individual variables
706 and feature families.

707 The final dataset contained 31,986 reads for training and 7,997 reads for test-
708 ing, with classes balanced (approximately 4,000 clean and 4,000 chimeric reads in
709 the test split).

710 4.1.1 Exploratory Data Analysis

711 An exploratory data analysis (EDA) was conducted on the extracted feature ma-
712 trix to characterize general patterns in the data and gain preliminary insight into
713 which variables might meaningfully contribute to classification. Histograms of key
714 features indicated that alignment-based variables showed clear class separation as
715 chimeric reads have higher frequencies of split alignments and broader long-tailed
716 distribution on soft-clipped regions (`softclip_left` and `softclip_right`). In
717 contrast, sequence-based variables such a microhomology length and k-mer di-
718 vergence displayed substantial overlap between classes, suggesting more limited
719 discriminative value. The complete set of histograms is provided in Appendix A.

720 As shown in Figure 4.1, the feature correlation heatmap shows that alignment-
721 derived features form a strongly correlated cluster, whereas sequence-derived fea-
722 tures show weak correlations with both the alignment-based features and with
723 one another. This heterogeneity indicates that no single feature family captures
724 all relevant signal sources.

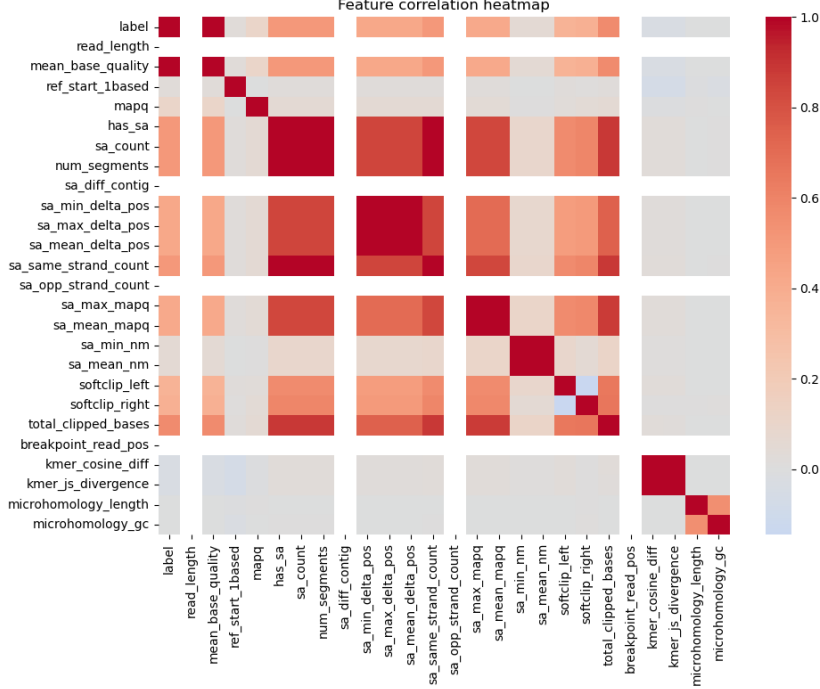


Figure 4.1: Feature correlation heatmap showing relationships among alignment-derived and sequence-derived features.

725 4.2 Baseline Classification Performance

726 Table 4.1 summarises the performance of eleven classifiers trained on the engi-
 727 neered feature set using five-fold cross-validation and evaluated on the held-out
 728 test set. All models were optimised using default hyperparameters, without ded-
 729 icated tuning.

730 The dummy baseline, which always predicts the same class regardless of the
 731 input features, achieved an accuracy of 0.50 and test F1-score of 0.67. This re-
 732 flects the balanced class distribution and provides a lower bound for meaningful
 733 performance.

734 Across other models, test F1-scores clustered in a narrow band between ap-
 735 proximately 0.74 and 0.77 and ROC–AUC values between 0.82 and 0.84. Gradi-
 736 ent boosting, CatBoost, LightGBM, XGBoost, bagging trees, random forest, and
 737 multilayer perceptron (MLP) all produced very similar scores, with CatBoost and
 738 gradient boosting slightly ahead (test F1 \approx 0.77, ROC–AUC \approx 0.84). Linear
 739 models (logistic regression and calibrated linear SVM) performed only marginally
 740 worse (test F1 \approx 0.74), while Gaussian Naive Bayes lagged behind with substan-
 741 tially lower F1 (\approx 0.65) despite very high precision for the chimeric class.

Table 4.1: Performance of baseline classifiers on the held-out test set.

model	test_accuracy	test_precision	test_recall	test_f1	test_roc_auc
dummy_baseline	0.500000	0.500000	1.000000	0.667000	0.500000
logreg_l2	0.789000	0.945000	0.614000	0.744000	0.821000
linear_svm_calibrated	0.789000	0.945000	0.614000	0.744000	0.820000
random_forest	0.788000	0.894000	0.654000	0.755000	0.834000
extra_trees	0.788000	0.901000	0.647000	0.753000	0.824000
gradient_boosting	0.802000	0.936000	0.648000	0.766000	0.840000
xgboost	0.800000	0.929000	0.650000	0.765000	0.839000
lightgbm	0.799000	0.926000	0.650000	0.764000	0.838000
catboost	0.803000	0.936000	0.650000	0.767000	0.839000
knn	0.782000	0.892000	0.642000	0.747000	0.815000
gaussian_nb	0.741000	0.996000	0.483000	0.651000	0.819000
bagging_trees	0.792000	0.900000	0.657000	0.760000	0.837000
mlp	0.789000	0.931000	0.625000	0.748000	0.819000

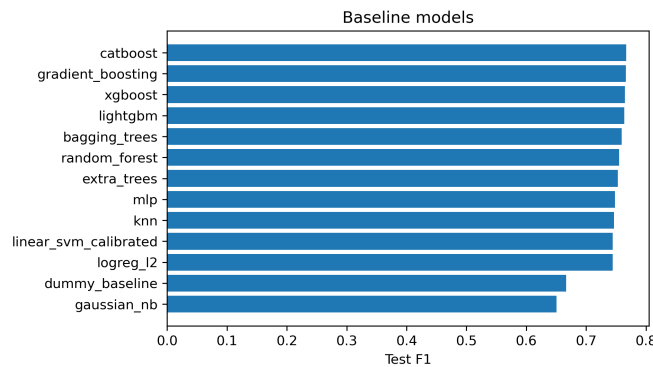


Figure 4.2: Test F1 of all baseline classifiers, showing that no single model clearly dominates and several achieve comparable performance.

742 4.3 Effect of Hyperparameter Tuning

743 To assess whether performance could be improved further, ten model families un-
744 derwent randomised hyperparameter search. The tuned metrics are summarised
745 in Table 4.2. Overall, tuning yielded modest but consistent gains for tree-based en-
746 sembles and boosting methods, while leaving linear models essentially unchanged
747 or slightly worse.

748 CatBoost, gradient boosting, LightGBM, XGBoost, random forest, bagging
749 trees, and MLP all experienced small increases in test F1 (typically $\Delta F1 \approx 0.002$ –
750 0.009) and ROC–AUC (up to $\Delta AUC \approx 0.008$). After tuning, CatBoost remained
751 the best performer with test accuracy 0.80, precision 0.92, recall 0.66, F1-score
752 0.77, and ROC–AUC 0.84. Gradient boosting achieved almost identical perfor-
753 mance (F1 0.77, AUC 0.84). Random forest and bagging trees also improved to
754 F1 scores around 0.76 with AUC ≈ 0.84 .

Table 4.2: Performance of tuned classifiers on the held-out test set.

model	test_accuracy	test_precision	test_recall	test_f1	test_roc_auc
logreg_l2_tuned	0.788000	0.946000	0.612000	0.743000	0.818000
linear_svm_calibrated_tuned	0.788000	0.944000	0.612000	0.743000	0.818000
random_forest_tuned	0.797000	0.915000	0.655000	0.763000	0.842000
extra_trees_tuned	0.794000	0.910000	0.652000	0.760000	0.837000
gradient_boosting_tuned	0.802000	0.928000	0.654000	0.767000	0.843000
xgboost_tuned	0.799000	0.922000	0.653000	0.765000	0.839000
lightgbm_tuned	0.801000	0.930000	0.651000	0.766000	0.842000
catboost_tuned	0.802000	0.924000	0.658000	0.769000	0.844000
bagging_trees_tuned	0.798000	0.922000	0.650000	0.763000	0.842000
mlp_tuned	0.790000	0.934000	0.625000	0.749000	0.821000

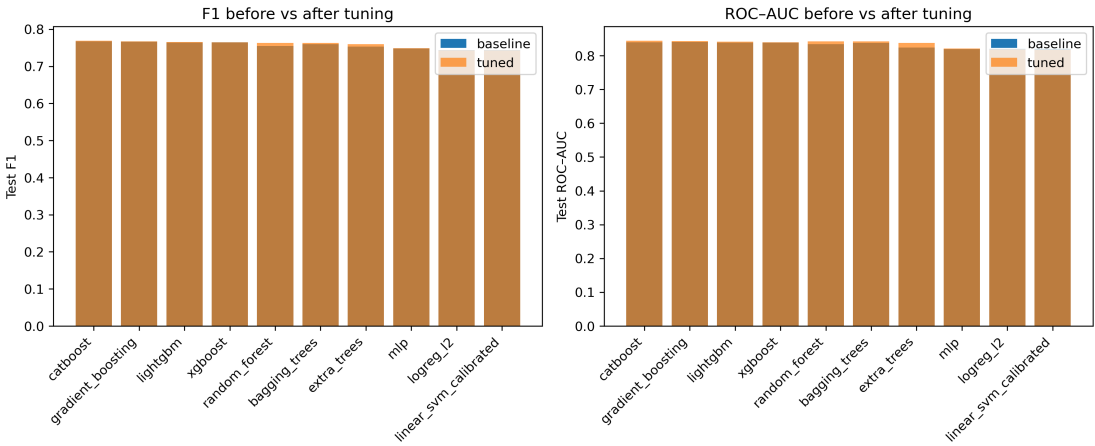


Figure 4.3: Comparison of test F1 (left) and ROC–AUC (right) for baseline and tuned models.

755 Because improvements are small and within cross-validation variability, tun-
 756 ing was interpreted as stabilising and slightly refining the models rather than
 757 completely altering their behaviour or their relative ranking.

758 4.4 Detailed Evaluation of Representative Mod- 759 els

760 For interpretability and diversity, four tuned models were selected for deeper
 761 analysis: CatBoost (best-performing boosted tree), scikit-learn gradient boost-
 762 ing (canonical gradient-boosting implementation), random forest (non-boosted
 763 ensemble baseline), and L_2 -regularised logistic regression (linear baseline). All
 764 models were trained on the engineered feature set and evaluated on the same
 765 held-out test data.

766 4.4.1 Confusion Matrices and Error Patterns

767 Classification reports and confusion matrices for the four models reveal consistent
768 patterns. CatBoost and gradient boosting both reached overall accuracy of ap-
769 proximately 0.80 with similar macro-averaged F1 scores (~ 0.80). For CatBoost,
770 precision and recall for clean reads were 0.73 and 0.95, respectively, while for
771 chimeric reads they were 0.92 and 0.66 ($F1 = 0.77$). Gradient boosting showed
772 nearly identical trade-offs.

773 Random forest attained slightly lower accuracy (0.80) and chimeric F1 (0.76),
774 whereas logistic regression achieved the lowest accuracy among the four (0.79)
775 and chimeric F1 (0.74), although it provided the highest chimeric precision (0.95)
776 at the cost of lower recall (0.61).

777 Across all models, errors were asymmetric. False negatives (chimeric reads
778 predicted as clean) were more frequent than false positives. For example, CatBoost
779 misclassified 1,369 chimeric reads as clean but only 215 clean reads as chimeric.
780 This pattern indicates that the models are conservative and prioritise avoiding
781 false chimera calls at the expense of missing some true chimeras.

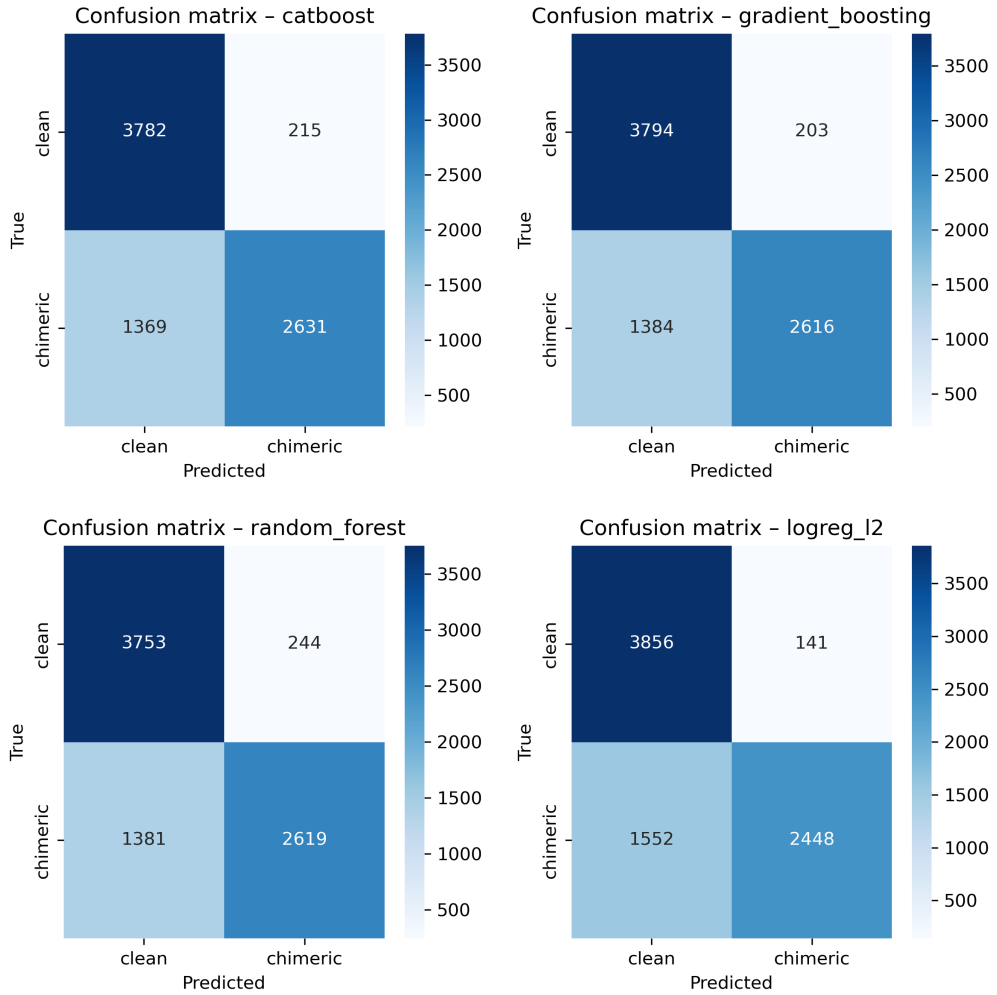


Figure 4.4: Confusion matrices for the four representative models on the held-out test set.

⁷⁸² 4.4.2 ROC and Precision–Recall Curves

⁷⁸³ Receiver operating characteristic (ROC) and precision–recall (PR) curves as
⁷⁸⁴ shown in Figure 4.5 further support the similarity among the top models. The
⁷⁸⁵ three tree-based ensembles (CatBoost, gradient boosting, random forest) achieved
⁷⁸⁶ ROC–AUC values of approximately 0.84 and average precision (AP) around 0.88.

787 Logistic regression performed slightly worse ($AUC \approx 0.82$, $AP \approx 0.87$) but still
788 substantially better than the dummy baseline.

789 The PR curves show that precision remains above 0.9 across a broad range
790 of recall values (up to roughly 0.5–0.6), after which precision gradually declines.
791 This behaviour indicates that the models can assign very high confidence to a
792 subset of chimeric reads, while more ambiguous reads can only be recovered by
793 accepting lower precision.

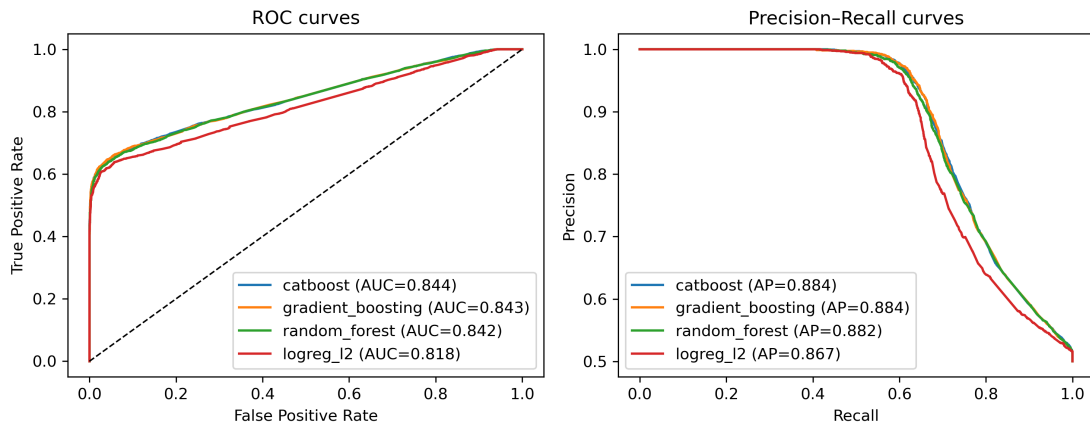


Figure 4.5: ROC (left) and precision–recall (right) curves for the four representative models on the held-out test set.

794 4.5 Feature Importance

795 4.5.1 Permutation Importance of Individual Features

796 To understand how each classifier made predictions, feature importance was quan-
797 tified using permutation importance. This analysis was applied to four represen-
798 tative models: CatBoost, Gradient Boosting, Random Forest, and L₂-regularized

799 Logistic Regression.

800 As shown in Figure 4.6, the total number of clipped bases consistently pro-
801 vides a strong predictive signal, particularly in Random Forest, Gradient Boosting,
802 and L₂-regularized Logistic Regression. CatBoost differs by assigning the highest
803 importance to k-mer divergence metrics such as `kmer_js_divergence`, which cap-
804 ture subtle sequence changes resulting from structural variants or PCR-induced
805 chimeras. Soft-clipping features (`softclip_left` and `softclip_right`) provide
806 more information around breakpoints, complementing these primary signals in all
807 models except Gradient Boosting. L₂-regularized Logistic Regression relies more
808 on alignment-based split-read metrics.

809 Overall, these results indicate that accurate detection of chimeric reads relies
810 on both alignment-based signals and k-mer compositional information. Explicit
811 microhomology features contribute minimally in this analysis, and combining both
812 alignment-based and sequence-level features enhances model sensitivity and speci-
813 ficity.

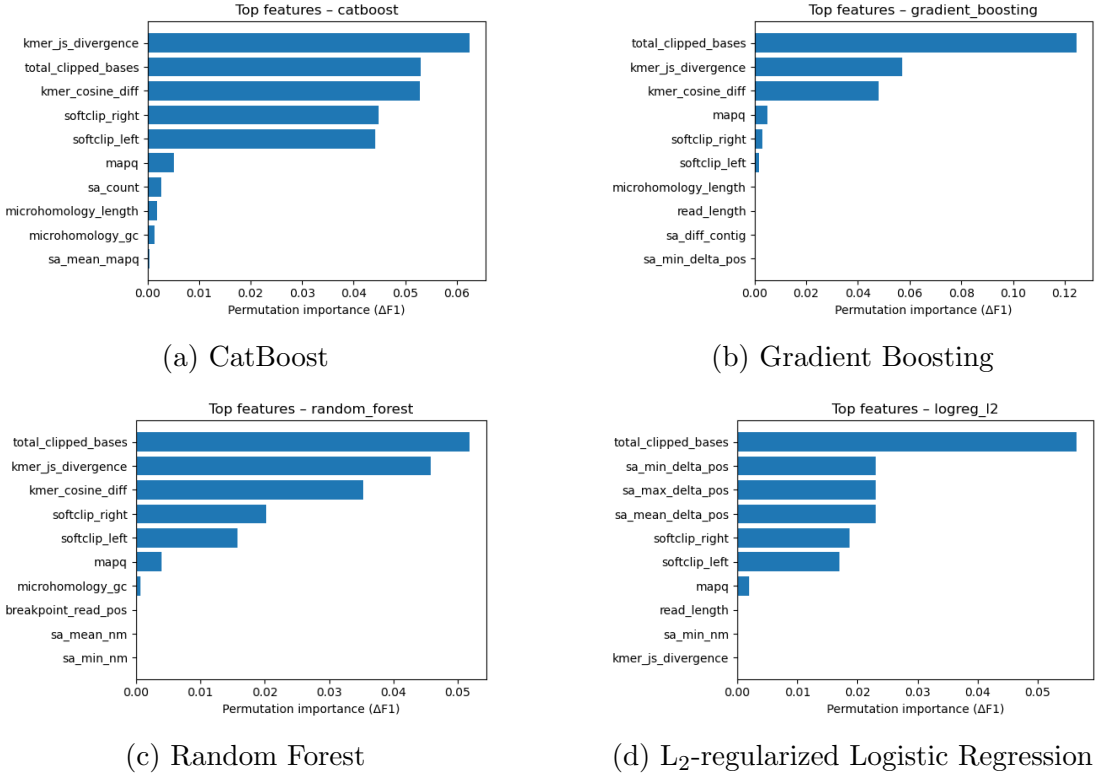


Figure 4.6: Permutation-based feature importance for four representative classifiers.

814 4.5.2 Feature Family Importance

815 To evaluate the contribution of broader signals, features were grouped into
 816 five families: SA_structure (supplementary alignment and segment met-
 817 rics, e.g., has_sa, sa_count, sa_min_delta_pos, sa_mean_nm, etc.), Clipping
 818 (softclip_left, softclip_right, total_clipped_bases, breakpoint_read_pos),
 819 Kmer_jump (kmer_cosine_diff, kmer_js_divergence), Micro_homology (microhomology_length,
 820 microhomology_gc), and Other (e.g., mapq).

821 Aggregated analyses reveal consistent patterns across models. In CatBoost,
 822 the Clipping family has the largest cumulative contribution (0.14), followed

823 by Kmer_jump (0.12), with Other features contributing minimally (0.005) and
824 SA_structure (0.003) and Micro_homology (0.003) providing minimal predictive
825 power. Gradient Boosting shows a similar trend, with Clipping (0.13) domi-
826 nating, Kmer_jump (0.11) secondary, and the remaining families contributing
827 negligibly. Random Forest integrates both Clipping (0.088) and Kmer_jump
828 (0.08) effectively, while SA_structure, Micro_homology, and Other remain minor
829 contributors. L₂-regularized Logistic Regression emphasizes Clipping (0.09)
830 and SA_structure (0.07), with Kmer_jump and Micro_homology having minimal
831 impact.

832 Both feature-level and aggregated analyses indicate that detection of chimeric
833 reads in this dataset relies primarily on alignment irregularities (Clipping) and
834 k-mer compositional shifts (Kmer_jump), which often arise from PCR-induced
835 template switching events, while explicit microhomology features contribute min-
836 imally.

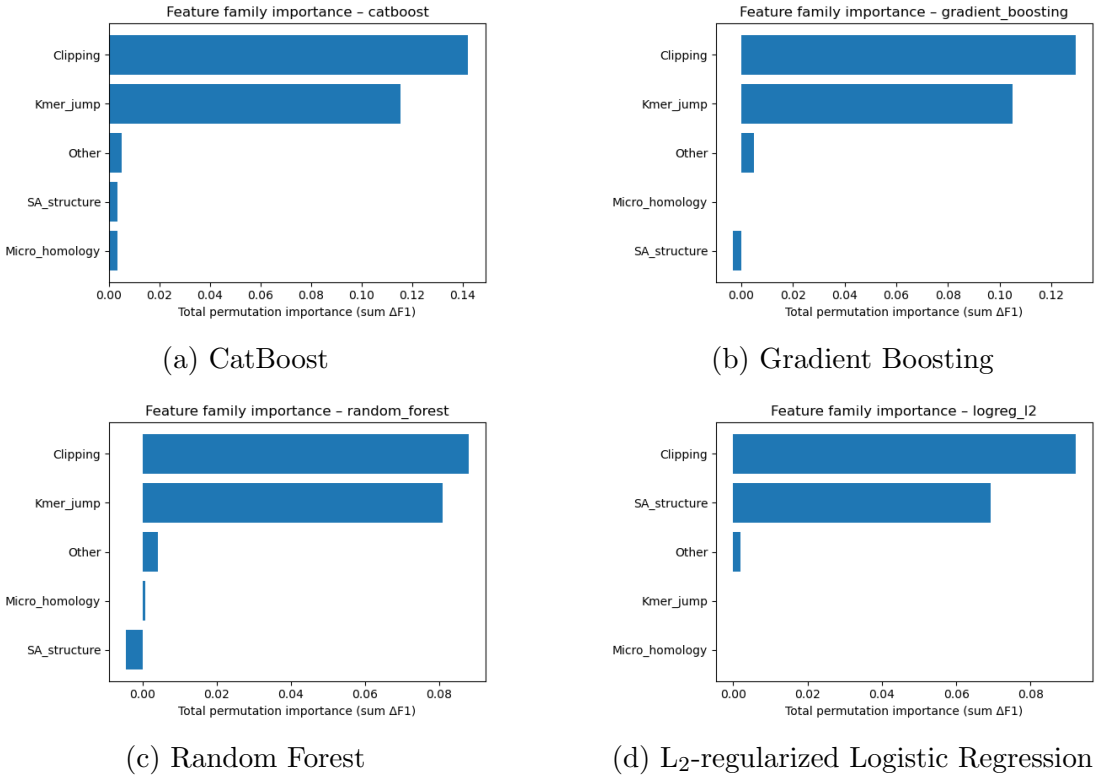


Figure 4.7: Aggregated feature family importance across four models.

837 4.6 Summary of Findings

838 All models performed substantially better than the dummy baseline, with test
 839 F1-scores around 0.76 and ROC-AUC values near 0.84. Hyperparameter tuning
 840 yielded modest improvements, with boosting methods, particularly CatBoost and
 841 gradient boosting, achieving the highest performance. Confusion matrices and
 842 precision-recall curves indicate that the models prioritize precision over recall for
 843 chimeric reads, minimizing false positives.

844 Feature importance analysis highlighted alignment breakpoints, such as clip-
 845 ping, and abrupt shifts in k-mer composition as the main contributors to predic-

846 tive power. Microhomology metrics and supplementary alignment features had
847 minimal impact. These findings suggest that alignment-based and k-mer-based
848 features alone are sufficient for training classifiers to detect mitochondrial PCR-
849 induced chimeric reads under the conditions tested.

850 **Appendix A**

851 **Exploratory Data Analysis**

852 **A.1 Histograms of Key Features**

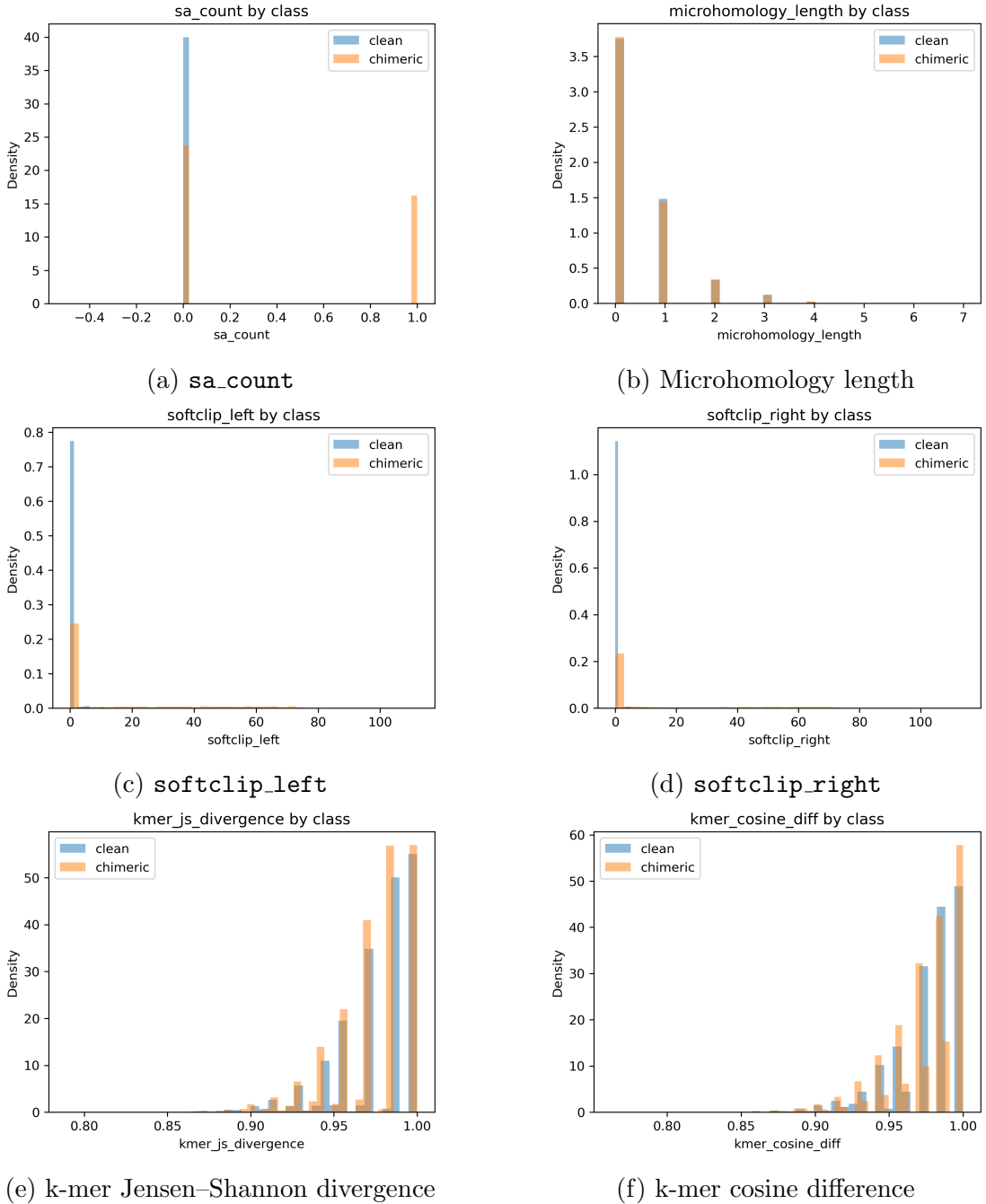


Figure A.1: Histogram plots of six key features comparing clean and chimeric reads.

⁸⁵³ References

- ⁸⁵⁴ Anderson, S., Bankier, A., Barrell, B., Bruijn, M., Coulson, A., Drouin, J., ...
⁸⁵⁵ Young, I. (1981, 04). Sequence and organization of the human mitochondrial
⁸⁵⁶ genome. *Nature*, *290*, 457-465. doi: 10.1038/290457a0
- ⁸⁵⁷ Arango, G., Garner, E., Pruden, A., Heath, L., Vikesland, P., & Zhang, L. (2018,
⁸⁵⁸ 02). Deeparg: A deep learning approach for predicting antibiotic resistance
⁸⁵⁹ genes from metagenomic data. *Microbiome*, *6*. doi: 10.1186/s40168-018
⁸⁶⁰ -0401-z
- ⁸⁶¹ Bentley, D. R., Balasubramanian, S., Swerdlow, H. P., Smith, G. P., Milton, J.,
⁸⁶² Brown, C. G., ... Smith, A. J. (2008). Accurate whole human genome
⁸⁶³ sequencing using reversible terminator chemistry. *Nature*, *456*(7218), 53–
⁸⁶⁴ 59. doi: 10.1038/nature07517
- ⁸⁶⁵ Boore, J. L. (1999). Animal mitochondrial genomes. *Nucleic Acids Research*,
⁸⁶⁶ *27*(8), 1767–1780. doi: 10.1093/nar/27.8.1767
- ⁸⁶⁷ Cameron, S. L. (2014). Insect mitochondrial genomics: Implications for evolution
⁸⁶⁸ and phylogeny. *Annual Review of Entomology*, *59*, 95–117. doi: 10.1146/
⁸⁶⁹ annurev-ento-011613-162007
- ⁸⁷⁰ Dierckxsens, N., Mardulyn, P., & Smits, G. (2017). Novoplasty: de novo assembly
⁸⁷¹ of organelle genomes from whole genome data. *Nucleic Acids Research*,

- 872 45(4), e18. doi: 10.1093/nar/gkw955
- 873 Edgar, R. C. (2016). Uchime2: improved chimera prediction for amplicon se-
874 quencing. *bioRxiv*. Retrieved from <https://api.semanticscholar.org/>
875 CorpusID:88955007
- 876 Edgar, R. C. (n.d.). *Uchime in practice*. Retrieved from https://www.drive5.com/usearch/manual7/uchime_practical.html
- 877 Edgar, R. C., Haas, B. J., Clemente, J. C., Quince, C., & Knight, R. (2011).
878 Uchime improves sensitivity and speed of chimera detection. *Bioinformatics*,
879 27(16), 2194–2200. doi: 10.1093/bioinformatics/btr381
- 880 Glenn, T. C. (2011). Field guide to next-generation dna sequencers. *Molecular
881 Ecology Resources*, 11(5), 759–769. doi: 10.1111/j.1755-0998.2011.03024.x
- 882 Gonzalez, J. M., Zimmermann, J., & Saiz-Jimenez, C. (2004, 09). Evalu-
883 ating putative chimeric sequences from pcr-amplified products. *Bioin-
884 formatics*, 21(3), 333-337. Retrieved from <https://doi.org/10.1093/bioinformatics/bti008>
885 doi: 10.1093/bioinformatics/bti008
- 886 Gray, M. W. (2012). Mitochondrial evolution. *Cold Spring Harbor perspectives
887 in biology*, 4. Retrieved from <https://doi.org/10.1101/cshperspect.a011403>
888 doi: 10.1101/cshperspect.a011403
- 889 Hahn, C., Bachmann, L., & Chevreux, B. (2013). Reconstructing mitochondrial
890 genomes directly from genomic next-generation sequencing reads—a baiting
891 and iterative mapping approach. *Nucleic Acids Research*, 41(13), e129. doi:
892 10.1093/nar/gkt371
- 893 Jin, J.-J., Yu, W.-B., Yang, J., Song, Y., dePamphilis, C. W., Yi, T.-S., & Li,
894 D.-Z. (2020). Getorganelle: a fast and versatile toolkit for accurate de
895 novo assembly of organelle genomes. *Genome Biology*, 21(1), 241. doi:
896 10.1186/s13059-020-02154-5
- 897

- 898 Judo, M. S. B., Wedel, W. R., & Wilson, B. H. (1998). Stimulation and sup-
899 pression of pcr-mediated recombination. *Nucleic Acids Research*, 26(7),
900 1819–1825. doi: 10.1093/nar/26.7.1819
- 901 Labrador, K., Agmata, A., Palermo, J. D., Ravago-Gotanco, R., & Pante, M. J.
902 (2021). Mitochondrial dna reveals genetically structured haplogroups of
903 bali sardinella (sardinella lemuru) in philippine waters. *Regional Studies in*
904 *Marine Science*, 41, 101588. doi: 10.1016/j.rsma.2020.101588
- 905 Li, H. (2018, 05). Minimap2: pairwise alignment for nucleotide sequences. *Bioin-*
906 *formatics*, 34(18), 3094-3100. Retrieved from <https://doi.org/10.1093/bioinformatics/bty191> doi: 10.1093/bioinformatics/bty191
- 907 Liang, Q., Bible, P. W., Liu, Y., Zou, B., & Wei, L. (2020, 02). Deepmi-
908 crobes: taxonomic classification for metagenomics with deep learning. *NAR*
909 *Genomics and Bioinformatics*, 2(1), lqaa009. Retrieved from <https://doi.org/10.1093/nargab/lqaa009> doi: 10.1093/nargab/lqaa009
- 910 Metzker, M. L. (2010). Sequencing technologies — the next generation. *Nature*
911 *Reviews Genetics*, 11(1), 31–46. doi: 10.1038/nrg2626
- 912 Mysara, M., Saeys, Y., Leys, N., Raes, J., & Monsieurs, P. (2015). Catch,
913 an ensemble classifier for chimera detection in 16s rrna sequencing stud-
914 ies. *Applied and Environmental Microbiology*, 81(5), 1573-1584. Retrieved
915 from <https://journals.asm.org/doi/abs/10.1128/aem.02896-14> doi:
916 10.1128/AEM.02896-14
- 917 Peccoud, J., Lequime, S., Moltini-Conclois, I., Giraud, I., Lambrechts, L., &
918 Gilbert, C. (2018, 04). A survey of virus recombination uncovers canon-
919 ical features of artificial chimeras generated during deep sequencing li-
920 brary preparation. *G3 Genes—Genomes—Genetics*, 8(4), 1129-1138. Re-
921 trieved from <https://doi.org/10.1534/g3.117.300468> doi: 10.1534/
922 923

- 924 g3.117.300468
- 925 Qin, Y., Wu, L., Zhang, Q., Wen, C., Nostrand, J. D. V., Ning, D., ... Zhou, J.
926 (2023). Effects of error, chimera, bias, and gc content on the accuracy of
927 amplicon sequencing. *mSystems*, 8(6), e01025-23. Retrieved from <https://journals.asm.org/doi/abs/10.1128/msystems.01025-23> doi: 10.1128/
928 msystems.01025-23
- 929
- 930 Qiu, X., Wu, L., Huang, H., McDonel, P. E., Palumbo, A. V., Tiedje, J. M., &
931 Zhou, J. (2001). Evaluation of pcr-generated chimeras, mutations, and het-
932 eroduplexes with 16s rrna gene-based cloning. *Applied and Environmental*
933 *Microbiology*, 67(2), 880–887. doi: 10.1128/AEM.67.2.880-887.2001
- 934 Ren, J., Song, K., Deng, C., Ahlgren, N., Fuhrman, J., Li, Y., ... Sun, F. (2020,
935 01). Identifying viruses from metagenomic data using deep learning. *Quan-*
936 *titative Biology*, 8. doi: 10.1007/s40484-019-0187-4
- 937 Rodriguez-Martin, B., Palumbo, E., Marco-Sola, S., Griebel, T., Ribeca, P.,
938 Alonso, G., ... Djebali, S. (2017, 01). Chimpipe: Accurate detection of
939 fusion genes and transcription-induced chimeras from rna-seq data. *BMC*
940 *Genomics*, 18. doi: 10.1186/s12864-016-3404-9
- 941 Rognes, T., Flouri, T., Nichols, B., Quince, C., & Mahé, F. (2016). Vsearch: a
942 versatile open source tool for metagenomics. *PeerJ*, 4, e2584. doi: 10.7717/
943 peerj.2584
- 944 Sedlazeck, F., Rescheneder, P., Smolka, M., Fang, H., Nattestad, M., von Haeseler,
945 A., & Schatz, M. (2018, 06). Accurate detection of complex structural
946 variations using single-molecule sequencing. *Nature Methods*, 15. doi: 10
947 .1038/s41592-018-0001-7
- 948 Sfeir, A., & Symington, L. S. (2015). Microhomology-mediated end joining: A
949 back-up survival mechanism or dedicated pathway? *Trends in Biochemical*

- 950 *Sciences*, 40(11), 701-714. Retrieved from <https://www.sciencedirect.com/science/article/pii/S0968000415001589> doi: <https://doi.org/10.1016/j.tibs.2015.08.006>
- 951
- 952
- 953 Vervier, K., Mahé, P., Tournoud, M., Veyrieras, J.-B., & Vert, J.-P. (2015,
954 11). Large-scale machine learning for metagenomics sequence classifica-
955 tion. *Bioinformatics*, 32(7), 1023-1032. Retrieved from <https://doi.org/10.1093/bioinformatics/btv683> doi: 10.1093/bioinformatics/btv683
- 956
- 957 Willette, D., Bognot, E., Mutia, M. T., & Santos, M. (2011). *Biology and ecology
958 of sardines in the philippines: A review* (Vol. 13; Tech. Rep. No. 1). NFRDI
959 Technical Paper Series. Retrieved from <https://nfrdi.da.gov.ph/tpjf/etc/Willette%20et%20al.%20Sardines%20Review.pdf>
- 960